HiSST: 3rd International Conference on
High-Speed Vehicle Science & Technology
14–19 April 2024, Busan, Korea

Off-Design Performance through Transient Simulations of an Expander-Type Air-Turbo-Rocket

K. Van den Borre[1], F. Pettinato[2], B. H. Saracoglu[3]

Abstract

Expander-type Air-Turbo-Rocket (ATR) engines combine the characteristics of rocket engines and conventional air-breathing Brayton cycles, which provide them with excellent performance in terms of specific thrust and impulse over a wide range of altitudes and flight Mach numbers. The maximum flight Mach number is extended compared to other turbine-based cycles by isolating the turbine from the hot air flow. This combination of properties makes them particularly well suited for high-speed supersonic aircraft or the air-breathing ascent stage of spaceplanes. This work examines the off-design behaviour of an ATR engine which previously has been studied using on-design component characteristics. This requires the application of control mechanisms to stabilize and regulate the engine under transiently varying flight conditions. The final model is used to examine the operability range of the ATR along the ascent trajectory of a Mach 5 aircraft, the engine throttle behaviour, and steep engine transients.

Keywords: *Air-Turbo-Rocket, Hydrogen, Cycle Analysis, Engine Control, ESPSS*

Nomenclature

Latin

ATR – Air-Turbo Rocket
SABRE – Synergetic Air-Breathing Rocket Engine
DMR – Dual Mode Ramjet
TSFC – Thrust Specific Fuel Consumption
F_u – Uninstalled Thrust
$\dot{m}$ – Massflow Rate
N – Rotational Speed in RPM
P_c – Combustion Chamber Total Pressure
MR – Mixture Ratio
I_{sp} – Specific Impulse
A_{th} – Nozzle Throat Area
PR – Pressure Ratio
H – Total Enthalpy
R – Ideal Gas Constant
LHV – Lower Heater Value

Greek

Π – Compression/Expansion Ratio
η – Isentropic Efficiency
γ – Heat Capacity Ratio

Other

$\tilde{}$ – Corrected Variable

1. Introduction

The strong compression provided by high-speed intakes leads to high thermal loads on the engine components, limiting the operability range of the turbomachinery in conventional Brayton cycles. Alternative cycles, such as the Air-Turbo-Rocket (ATR), aim to address this issue by removing the turbine from the hot airflow path, which eliminates the metallurgic limits. In doing so the operability range of the turbine-based cycle can be extended to approximately Mach 5. As the ATR engine combines characteristics of both the rocket engines and turbine-based cycles, they exhibit some unique performance characteristics, such as a high specific impulse, thrust-to-weight ratio, and specific thrust for a wide range of altitudes

[1] *von Karman Institute for fluid dynamics, Waterloosesteenweg 72, 1640 Sint-Genesius-Rode, karel.vandenborre@vki.ac.be*
[2] *von Karman Institute for fluid dynamics, Waterloosesteenweg 72, 1640 Sint-Genesius-Rode, federico.pettinato@vki.ac.be*
[3] *von Karman Institute for fluid dynamics, Waterloosesteenweg 72, 1640 Sint-Genesius-Rode, bayindir.saracoglu@vki.ac.be*

and flight Mach numbers [1, 2]. This makes them particularly attractive for high-speed aircraft and air-breathing ascent stages for spaceplanes.

Multiple subtypes of ATR engines exist. The precooled ATR extends the operational envelope by cooling down the air shortly after it enters the intake. The heat recovered during this process, possibly supplemented with additional heat captured from the combustion chamber, is used to drive the turbine powering the air compressor. Examples of this cycle are the SABRE [3] and Scimitar [4] engines, both under development by Reaction Engines Limited. Another subtype is the expander type ATR, where a high-enthalpy fuel flow is expanded to drive the turbine powering the air compressor. In this case, the heat pick-up by the fuel usually occurs by heat exchangers placed after or at the combustion chambers. An example of the expander-type ATR is the ATREX engine, studied at JAXA [5].

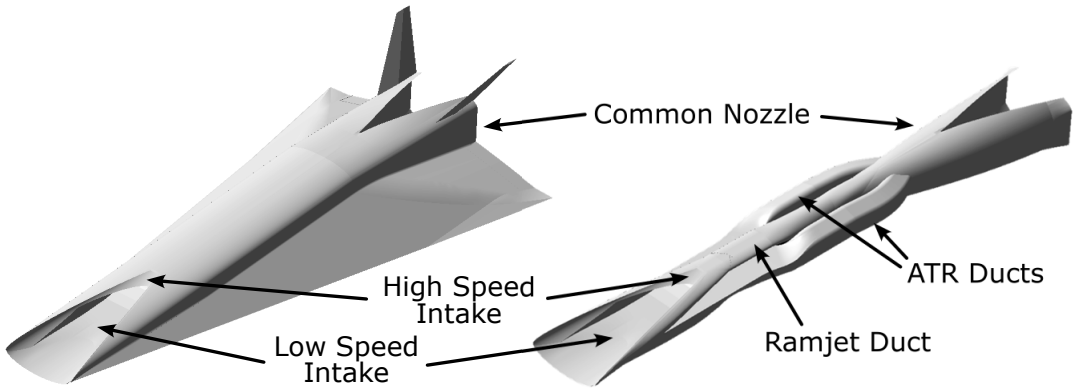

Fig 1. An external view of the MR 2.4 vehicle, together with the overall layout of the combined cycle propulsion plant.

During the LAPCAT I/II and STRATOFLY projects [6–8], a highly integrated combined cycle propulsion system was designed for a supersonic passenger transport aircraft, traveling at Mach 8 and 35 km of altitude (see figure 1). This propulsion system consists of a dual-mode ramjet to power the aircraft during cruise and 6 ATR expander-type engines that propel the aircraft during take-off, climb, and acceleration. This propulsion system is also used to power the MR5 concept under investigation by the follow-up MORE&LESS project, which shares the same root waverider vehicle design, albeit sized to cruise at a lower Mach number of 5, and a lower altitude of 25 km [9]. In the ATR expander engine, depicted schematically in figure 2, the freestream air is first subjected to a compression in the intake, before it passes through a set of counter-rotating fans which delivers the remaining compression required. The liquid hydrogen fuel stored cryogenically in the fuel tanks at 22 K and 3 bar [10] is pumped through a set of heat exchangers at the nozzle and combustion chamber, where they pick up heat while cooling the aforementioned components down. The resulting high-temperature, high-pressure hydrogen flow is then used to drive two hydrogen turbines which drive the hydrogen turbopump and counter-rotating fans. Afterwards, the air and fuel react in the combustion chamber where they expand before being ejected through a converging-diverging nozzle shared with the DMR engine.

While studies for the steady thrust of the total combined cycle engine, including the DMR, have been performed in the past [11–13], the present work focuses on the uninstalled ATR only to examine the off-design behavior and engine control strategy along the ascent stage of the vehicle. The engine is simulated with a transient model, which is exploited to investigate the engine stability limits along the flight trajectory and a practical implementation of engine throttling. The transient model further allows the investigation of the engine response to fast changes in engine control inputs and changes in flight conditions.

2. Methodology

2.1. Modelling Tools

The simulations are performed using EcosimPro coupled with the ESPSS library. EcosimPro is a multi-disciplinary object-oriented software package aimed at modeling continuous systems [14]. A model of a full system is created by assembling multiple individual components, each containing a mathematical description of their behavior. By connecting the components and providing the required boundary conditions, a closed system of differential equations is created that is solved using the Differential-Algebraic System Solver (DASSL) [15], which employs an implicit Newton-Raphson method. The time derivative is replaced with a backward differentiation of order k, which together with the timestep Δt varies during runtime based on the evolution of the solution. This allows for efficient simulation of problems containing both fast and slow variations in time. The European Space Propulsion System Simulation (ESPSS) library contains components for the simulation of spacecraft propulsion systems [16]. This includes databases for fluids, combustion chambers, turbomachinery, nozzles, and so forth. The combustion process is solved with the minimum free Gibbs energy approach using the CEA solver [17]. The air and combustion gasses are represented as mixtures of perfect gasses, while the hydrogen is considered a real fluid, with its fluid properties being interpolated from REFPROP tabulated data [18].

2.2. Steady on-design engine sizing

In previous studies, the ATR engine in question has been examined in multiple phases. In the first phase, a parametric cycle analysis was performed to identify critical engine design parameters, and how these lead to certain design trade-offs [1, 19]. The critical design parameters consisted of fan pressure ratio, mixture ratio, regenerator pressure loss, and heat pick-up. It was found the performance in terms of specific thrust and specific impulse is only dependent on the fan pressure ratio, mixture ratio, and flight regime. A design compromise was identified which states that to reduce the turbine expansion ratio (which correlates to turbine weight), the heat pick-up needs to be increased (which would lead to a heavier heat exchanger and larger pressure drop). This was used as a basis to size the heat exchangers, inlet, and nozzle, which allowed for an optimisation of the fuel consumption at several points along the flight trajectory [12] using a meta-model assisted differential-evolution approach [20] with the mixture ratio $MR = \dot{m}_{air}/\dot{m}_{fuel}$, combustion pressure ($P_c$), and nozzle throat area (A_{th}) as optimisation variables. The results of this optimisation, which includes the optimal value of the optimisation variables, uninstalled thrust output (F_u), and fuel consumption ($\dot{m}_{fuel}$), can be seen in Fig 3.

Fig 4a shows all the explored individuals for the optimisation of a single point of the trajectory at a flight velocity of Mach 0.75. This shows the algorithm converges to the point of minimum fuel consumption, where the minimum thrust requirement can be met. The red line on the same figure shows a Pareto front of all non-dominated individuals in the F_u - $\dot{m}_{fuel}$ space, which defines the ideal throttle curve,

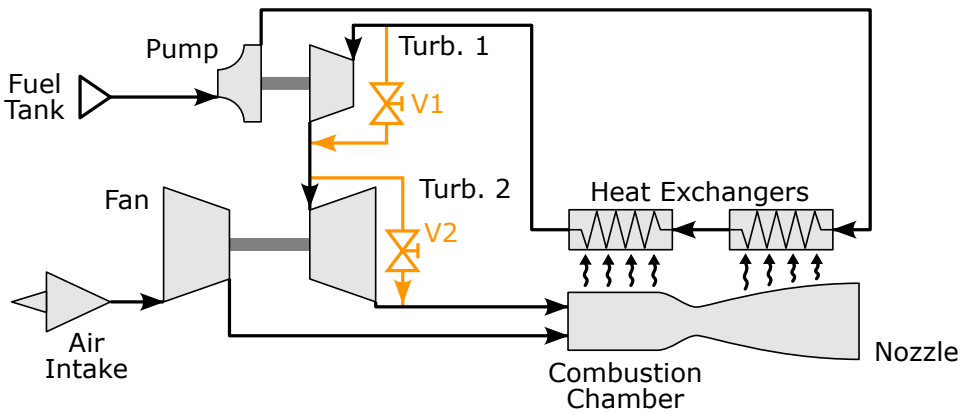

Fig 2. Schematic overview of the ATR engine, with the engine control valves implemented for off-design simulation indicated in orange.

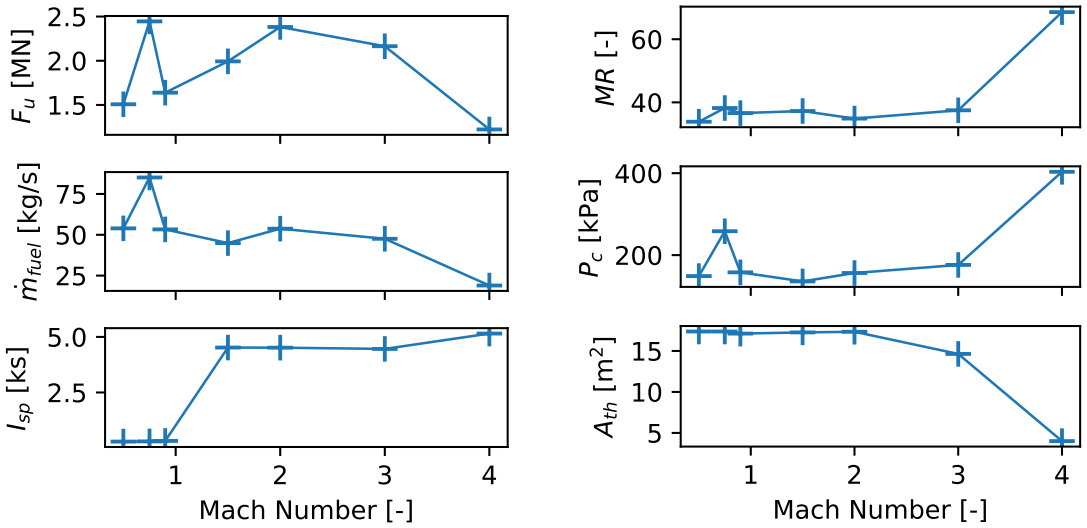

Fig 3. The results of the trajectory optimisation. On the left are the engine outputs and on the right are the optimised throttle variables.

where the optimal setting for P_c, A_{th}, MR is known for a given F_u. The resulting throttle curve can be seen in Fig 4b, where the evolution of the throttle variables as a function of the thrust output is depicted. The goal of the original work [12] leading to Fig 4a was to perform a single-point optimisation, which is in actuality not suited for a proper Pareto front generation. This manifests itself as clustering of the points along the trajectory, with regions far from the found optimum point being underrepresented. To provide a cleaner Pareto front, with more evenly spaced points, and an overall better performance, a multi-objective optimisation should be performed with the thrust output and fuel flow as optimisation objectives using, for example, the NSGA-II algorithm [21]. To improve the smoothness of the throttle curve for the purpose of demonstrating the capabilities of the off-design model, a polynomial regression of order 4 with a Huber regressor is performed. The Huber regressor has the advantage of not being heavily influenced by outliers, while still keeping their effect into consideration [22].

In the previous work, the off-design behavior of the injectors, heat exchangers, inlet, and nozzle was studied extensively [11], but not the off-design behavior of the turbomachinery. For the turbomachinery, the adiabatic efficiency was set to a fixed value and the turbine/compressor matching was only performed for the power balance, not for the spool speeds. As a result, the combination of throttle parameters P_c, A_{th}, and MR can be freely set along the entire flight trajectory, without considering whether this is a stable configuration and which practical implementation can meet these requirements. In ATR engines, the fan shaft power is delivered independent of the fan performance, which implies stability is not inherently guaranteed, as opposed to more conventional Brayton-based cycles, which has been discussed for gas-generator type ATR engines by Bossard and Thomas [23].

2.3. Off-design component behaviour

As discussed in section 2.2, the previous works performed all simulations in an "on-design" mode, where the compression ratio of the fans, mixture ratio, and combustion chamber throat area could be freely set along the entire flight trajectory. The alternative is to include performance maps of the turbomachinery components, which are represented by beta-N maps. These describe the component adiabatic efficiency, corrected mass flow rate, and compression ratio as a function of the corrected rotational speed and a mathematical beta parameter dividing the constant corrected rotational speed lines in equal parts (see equations 1 and 2). Ideally, the map corresponding with the actual machine should be used for the most reliable results, which is not possible during the preliminary design phase, as the real turbomachinery does not yet exist.

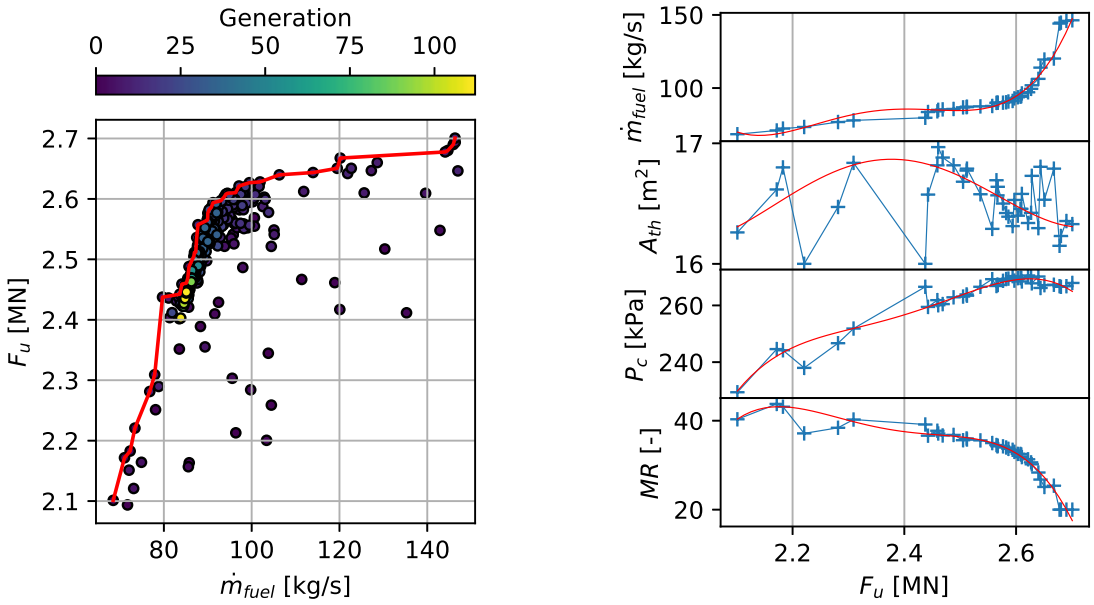

(a) All explored points during the cycle optimisation at Mach 0.75. The Pareto-front is indicated in red.

(b) Evolution of the throttle parameters along the Pareto front. Red shows a polynomial regression of order 4.

Fig 4. The engine throttle curve is extracted from the Pareto-front of the optimisation results.

$$\Pi(\tilde{N},\beta) = \begin{cases} p_{t,out}/p_{t,in} & \text{compressor} \\ p_{t,in}/p_{t,out} & \text{turbine} \end{cases} \tag{1}$$

$$\eta(\tilde{N},\beta) = \begin{cases} \Delta H_s/\Delta H & \text{compressor} \\ \Delta H/\Delta H_s & \text{turbine} \end{cases} \tag{2}$$

$$\tilde{\dot{m}}(\tilde{N},\beta) = \frac{\dot{m}\Theta}{\delta} \tag{3}$$

with:

$$\delta = p_{in}/p_{ref}$$
$$\Theta = (R_g T)_{in}/(R_g T)_{ref}$$
$$\tilde{\dot{m}} = \frac{\dot{m}\sqrt{\Theta}}{\delta}$$
$$\tilde{N} = \frac{N}{N_d\sqrt{\Theta}}$$
$N_d =$ Design rotational speed

To solve this issue, maps of related turbomachinery from the literature are used, which are then rescaled to fit the requirements of the new preliminary machine. These scaling factors are defined by equations 4 to 6. For the counter-rotating fans, the NASA-CR-174645 Booster Map is used [24]. For both turbines powering the fuel pump and counter-rotating fans respectively, the NASA-TM-83655 radial turbine map is used [25]. For the fuel pump itself, a generic description is used based on non-dimensionalised tabulated data for the pump head and torque requirement at the shaft [26].

$$\Pi_s(\tilde{N},\beta) = 1 + k_\Pi \cdot (\Pi_{orig}(\tilde{N},\beta) - 1) \tag{4}$$

$$\tilde{\dot{m}}_s(\tilde{N},\beta) = k_m \cdot \tilde{\dot{m}}_{orig}(\tilde{N},\beta) \tag{5}$$

$$\eta_s(\tilde{N},\beta) = k_\eta \cdot \eta_{orig}(\tilde{N},\beta) \tag{6}$$

with subscripts:

s = scaled map
$orig$ = original unscaled map

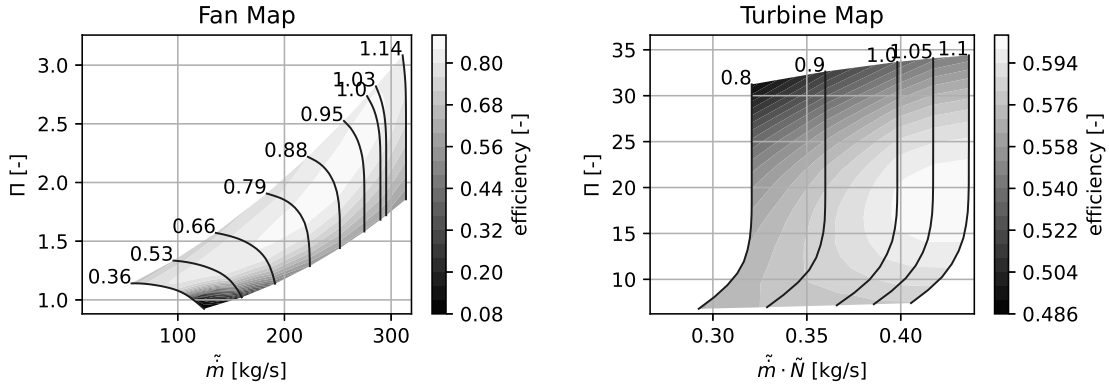

Fig 5. Unscaled maps used for the fans (left) and turbines (right).

2.4. Proposed control strategy

In the transient model with turbomachinery speed matching, the degrees of freedom to impose the throttle parameters P_c and MR are no longer available. Instead, P_c and MR are determined by the equilibrium resulting from the matching process. In order to set these throttle parameters to their desired values, as determined in section 2.2, these degrees of freedom need to be restored. This is possible by introducing a series of valves, represented in orange in Fig 2. V1, alias the pump bypass valve, bypasses turbine 1, powering the pump. By opening this valve the turbine power output is lowered by reducing the mass flow rate and by reducing the expansion ratio. This slows down the connected pump, lowering the fuel flow rate, and in turn, increasing the MR. With V2, alias the fan bypass valve, part of the high-enthalpy flow bypasses turbine 2, powering the fan. By doing so, the mass flow rate through and the expansion ratio across the turbine are lowered, decreasing the power output. This lowers the pressure ratio and mass flow rate of the connected fan, which determines P_c. In this way, a control strategy is created where MR is controlled by V1 and P_c is controlled by V2. It is important to note that the control action of the valves extends beyond their respective throttle variable. For example, opening V1 will lower the power output to the pump, which next to increasing MR as intended, will also decrease the pressure ratio of the pump. This leads to a lower expansion ratio in both turbines, lowering the power input to the fan, in turn decreasing P_c. This phenomenon is called cross-coupling and could pose issues for the overall controllability of the system. Methods to properly handle cross-coupling exist, detailed in the work by Sivadasan et al. [27] for example. As no issues related to cross-coupling were encountered in the present work, these are not implemented to limit the overall system complexity. The precise position of the valves is controlled using two independent PI controllers. The proportional gain and integral time constants have been set using manual tuning until a stable control with a reasonable response time was achieved. The popular heuristic Ziegler-Nichols method [28] was attempted, but due to the strong non-linear behaviour of the system it did not yield a stable engine control over the full throttle and flight condition range.

3. Results

Using the sized system with reasonable controller tuning, three different experiments are conducted. In the first experiment, the engine is throttled up from 350 to 450 kN of thrust. In the second experiment, a section of the optimised mission trajectory is simulated to investigate the engine's operational limits. The third experiment looks at the transient response after imposing steep throttle changes.

3.1. Engine throttling

In this section, the on-design throttle curve resulting from the steady optimisation in section 2.2 is replicated using the transient off-design engine model. Here, the intent is to linearly change the thrust output of the engine by imposing the throttle parameters according to Fig. 4b. The experiment is conducted over 20000 seconds simulated time, ensuring the effect of the control lag is minimal and the engine operates in a quasi-steady-state. This comes to no additional computational cost, as the DASSL algorithm automatically enlarges the timestep. Figure 6 compares the throttle parameters and engine performance for the steady and transient models. This comparison shows that the control system is able to properly set the throttle parameters to the required values over the investigated throttle range. Even when the throttle parameters match, the off-design engine performance is different from the on-design performance, which is in line with the initial expectations. The fuel flow provides the best match. This can be related to the fact that the fuel flow rate is described by MR, which is imposed, and the airflow rate. The latter is governed by the chocked flow equation (eq. 7), where the main parameters are the upstream total pressure and temperature.

$$\dot{m} = \frac{A \cdot p_t}{\sqrt{T_t}} \sqrt{\frac{\gamma}{R}} M \left(1 + \frac{\gamma - 1}{2} M^2\right)^{-\frac{\gamma+1}{2(\gamma-1)}} \tag{7}$$

The total pressure is imposed through the controller and the deviation in total temperature is mainly caused by the fan isentropic efficiency and the heat capture rate in the combustion chamber. The latter does change with respect to the on-design case, as for this isolated ATR case, the nozzle and heat exchanger topology are greatly simplified, as detailed in 2.2.

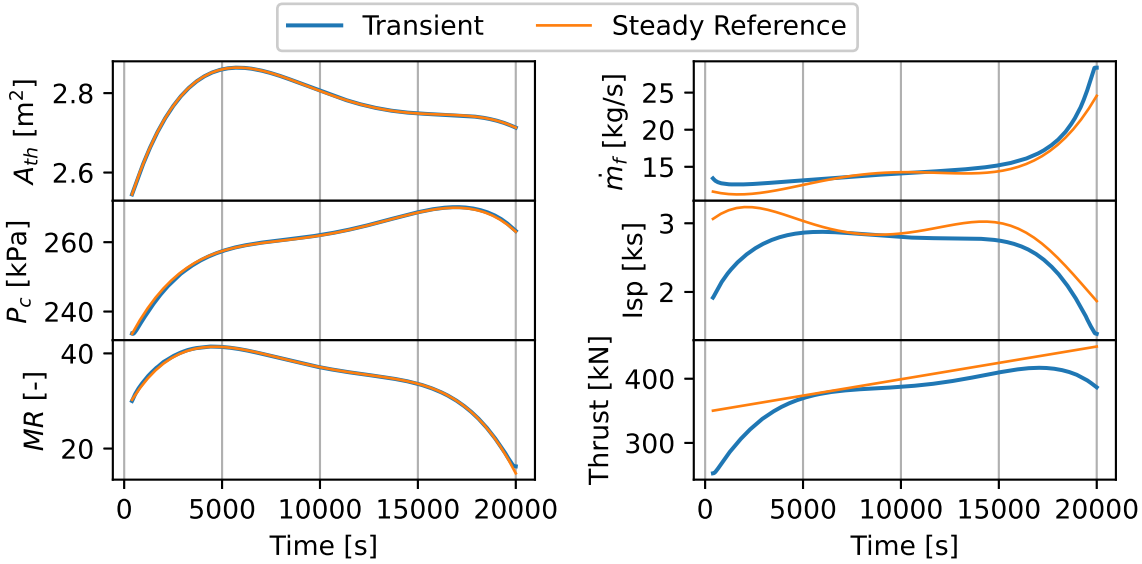

Fig 6. results of the throttle curve experient

A bigger deviation can be seen in the engine thrust output, which shows an evolution that is far from the expected linear behaviour. This deviation can be explained by the changes in the heat exchanger

and nozzle topology, the off-design behaviour of the turbomachinery, and the additional losses imposed by the bypass valves. However, the key result from this experiment is that controllability is observed by imposing the throttle variables using the implemented bypass valves. Despite the differences, some engine trends are confirmed. For example, at high throttle settings, a high fuel flow is required which leads to a rich combustion, wasting a large portion of the potential chemical energy, ultimately leading to a sharp decrease in I_{sp}.

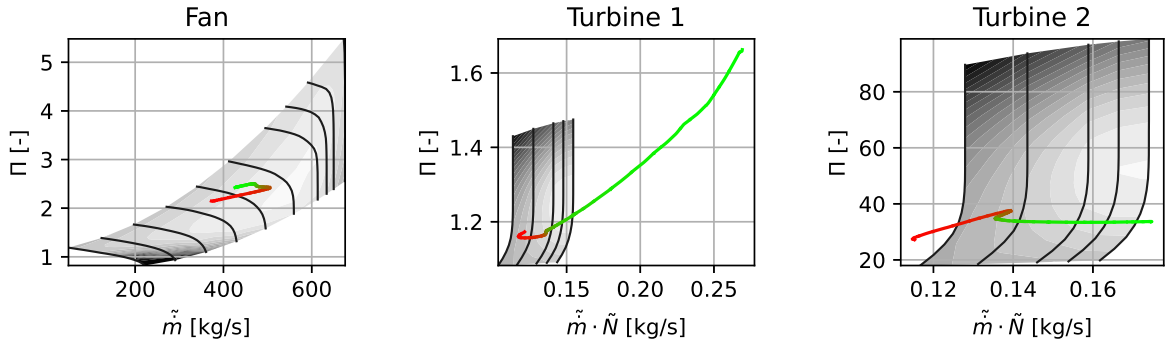

Fig 7. Locus of the turbomachinery operating points for the throttle experiment. The color goes from red to green as time progresses.

Figure 7 shows the locus of the turbomachinery operating points on their respective maps. The color of the locus indicates the time of the simulation, with red representing the start of the simulation (low throttle setting) and green representing the end (high throttle setting). This shows that despite our best efforts to scale the maps to include as many of the trajectory points as viable, it was not possible to keep all the operating points on the turbomachinery maps during throttling. For Turbine 2, there are two small excursions towards both the high and low ends of the throttle curve, the limiting factor seems to be the corrected mass flow rate range. For Turbine 1, a large excursion is found at high throttle settings towards the high corrected mass flow range. The expansion ratio also exceeds the limit of the map, although this could realistically be resolved by adjusting the scaling. For the Fan, the operating point lies well within the boundaries of the map. To ensure wider operability of the turbines, the scaling procedure of 2.3 can no longer be used, as this methodology is unable to extend the range for both high and low mass flow rates. Either another scaling needs to be implemented, or maps of more representative machines need to be sourced.

3.2. Step response

The main feature of a transient model is the ability to explore quick unsteady engine behaviour. In this section, this is demonstrated by performing two steps of the thrust output at Mach 0.75 flight conditions. The first is a step up from 350 kN to 375 kN, and the second step is the inverse. This step is achieved by directly imposing the throttle parameter values as input to their respective controllers, which is shown in orange in Fig. 9. This figure also shows the actual response in blue and the valve opening positions on top. When looking at the upward step, P_c needs to increase and MR needs to drop. To accomplish both these actions, both valves should close, providing more power to the turbine. This is also the immediate effect seen in the valves. However, the immediate response of P_c and MR are in opposition to the expected response. This is because the pressure ratio across the turbomachinery reacts faster than the mass flow rate, as the change in mass flow rate is limited by the flow and spool inertia. This results in a large but short pressure peak being generated across the turbomachinery components, leading to a peak in upstream pressure, right after the heat exchangers, and a drop in downstream pressure, which is the chamber pressure P_c. Closing both valves at the same time also leads to an increased flow resistance across the turbine-valve system, lowering the fuel flow rate, which leads to an increase in MR until the valves start opening again. For both P_c and MR overshoot above their setpoint can be seen, which recovers until no steady-state error remains. This overshoot could be avoided with a better tuning of

the PI controller, or by including a derivative action, leading to PID control. For the down-throttle step, a similar, reverse behaviour can be seen. The key difference is that the opening area of the valve is not limited, as such the valve position does not saturate, which it did for the throttle-up maneuver where the valves fully closed. This could lead to large valve opening positions, potentially pushing the engine to a non-sustainable configuration, crashing the solver. This has been observed in simulations where the proportional gain of the controllers was too large. Ultimately, the overshoot in throttle parameters manifests itself as an overshoot in the thrust output and I_{sp}, which can be seen in Fig. 8.

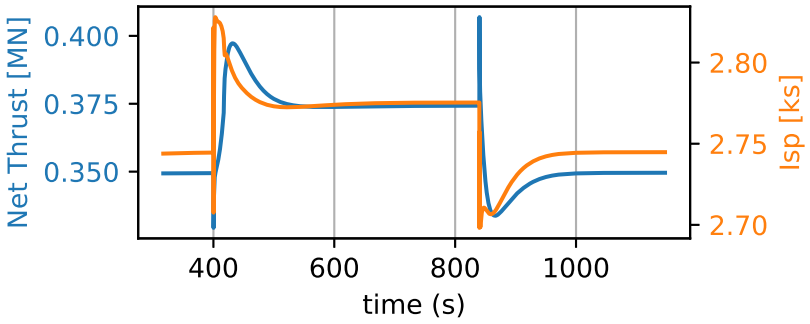

Fig 8. Step response of the thrust output and specific impulse.

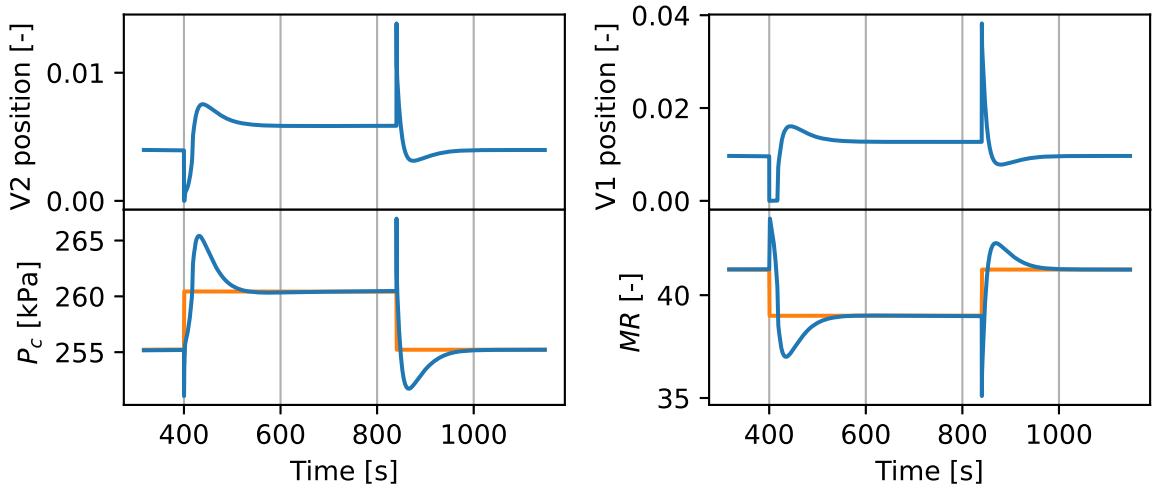

Fig 9. The bottom plots show the response of the engine throttle parameters (blue) for a step input (orange). The top plots show the response of the control valves.

Figure 10 shows the locus of the turbomachinery operating points, as the engine reacts to a step input along the throttle curve. The green curve indicates up-throttling and the red curve indicates down-throttling. A hysteresis effect is visible in all turbomachinery components, caused by the fact that the pressure differences are faster acting than changes in the rotational speed of the turbomachinery. This is especially clear on the map of Turbine 2. Here, when the step-up is initiated, the pressure quickly adapts to the new situation, with a sudden increase of Π. This can be seen as an upward movement of the operating point, parallel to the constant speed lines (black). This higher pressure ratio increases the power availability in the spool, speeding it up, which can be seen by the movement of the operating point to the right, towards higher constant speed lines. A similar behaviour manifests itself during down-throttling. The Fan also shows this clear behavior of first moving parallel to the constant speed lines,

before slowly settling to the new operating point at a different rotational speed. It is also interesting to note that contrasted to conventional turbojet engines, an upward thrust step is beneficial to the compressor stall margin, while a downward step is detrimental.

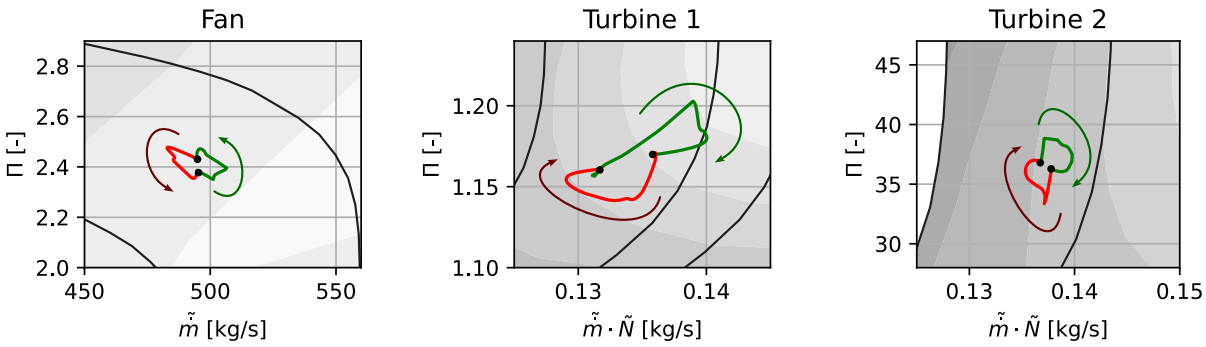

Fig 10. Locus of the turbomachinery operating points for the step experiment. The green curve indicates the up-throttle step and the red curve the down-throttle step.

3.3. Off-Design Performance During Flight

In this section, the transient model is used to assess the off-design engine performance and limitations for the optimised mission discussed in section 2.2. For each point along the trajectory, the engine throttle parameters found during the steady optimisation are given as set-point to their respective PI-controllers. In between the steady points, a linear interpolation is used. As the main goal of the current experiment is to study the engine performance and turbomachinery limits, the transient and control lag effects are eliminated by increasing the simulation time to 60000 seconds.

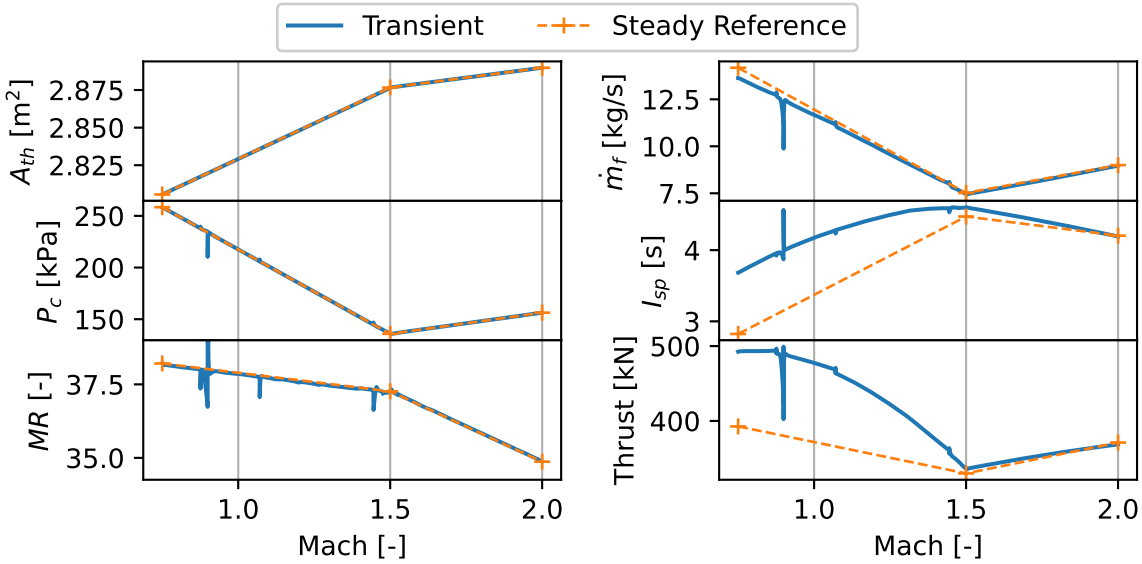

Fig 11. The throttle parameters and engine outputs for the section in the flight trajectory spanning from Mach 0.75 to Mach 2.

The results presented in Fig. 11 show the evolution from Mach 0.75 to Mach 2. When moving beyond this range, the engine hits the operability limits and the controllers fail to meet both the P_c and MR setpoints. The cause of this limited operational range is still under investigation. Within the range of

Mach 0.75 to Mach 2, the throttle parameters match well. The fuel flow is in line with the expected behaviour, as is the thrust output for a Mach number higher than 1.5. At a Mach number of 0.75, the thrust is overestimated compared to the steady reference result. A possible cause for this thrust difference is the simplifications to the nozzle and heat exchanger topology compared to the original steady model, which has been applied to study the effect of a single ATR instead of the whole combined cycle propulsion plant.

Figures 12 and 13 show the Sankey diagrams for the ATR operating at the optimal point for Mach 0.75 and Mach 2.00 respectively. These diagrams are a powerful tool to provide insight into the energy flow and conversion within the system. The first thing to note is the low overall efficiency of the engine, as defined by Eq. 8. For a flight speed of Mach 0.75, η_o is equal to 8.0 %, which increases to 20 % for a flight speed of Mach 2. This is in line with earlier findings of Miranda et al. [1], who derived similar values when performing a parametric analysis for a highly idealised ATR engine operating at Mach 2. The flight velocity being present in the numerator of Eq. 8 is part of the reason for the apparent increase in overall efficiency as the flight velocity increases. Another metric confirming more efficient engine operation at higher flight velocities is the I_{sp}, depicted in Fig. 11.

$$\eta_o = \frac{F_u \cdot v_{flight}}{LHV \cdot \dot{m}_{fuel}} = \frac{I_{sp} \cdot v_{flight}}{LHV} \tag{8}$$

The Sankey diagrams illustrate the relative magnitude of the energy flows throughout the engine. The pump power for example is an order of magnitude smaller than the fan power, which manifests itself as a much larger expansion ratio in turbine 2 than in turbine 1, as the turbines are placed in series (see for example Fig. 7). It also shows the energy used by the hydrogen cycle is modest relative to the total energy released during the combustion process, certainly when compared to conventional turbojet and turbofan engines. This is mainly caused by the modest compression ratios presented by the fans, which are in the vicinity of 2, and by the fact that the heat capture rate is limited by the heat exchanger technology and weight.

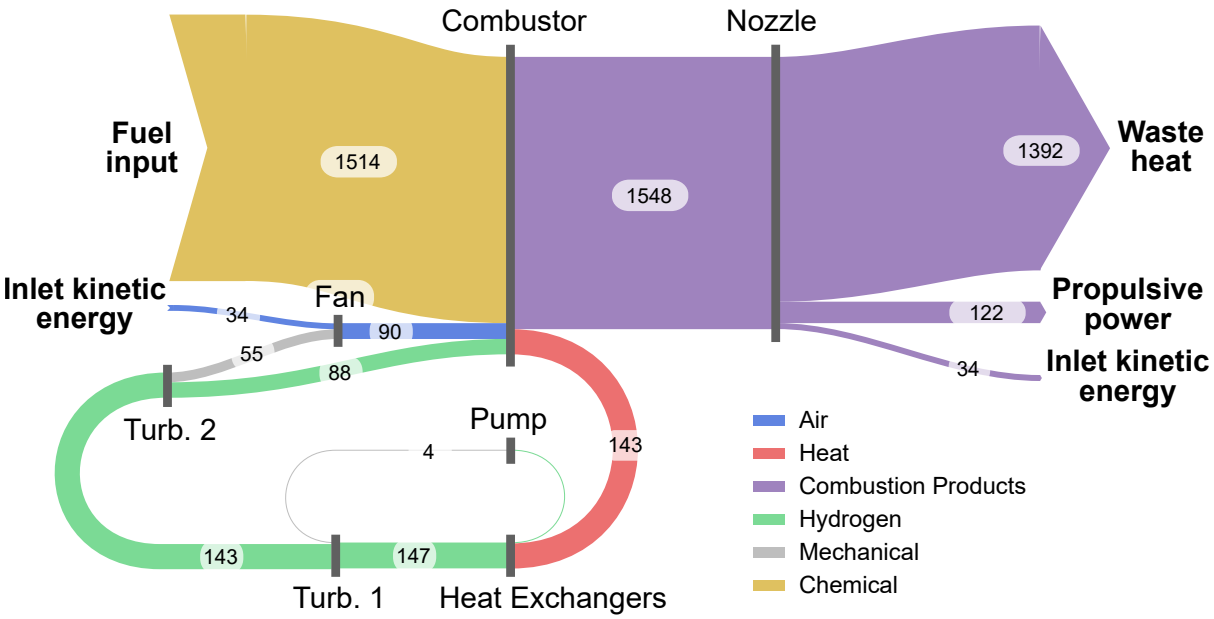

Fig 12. Sankey diagram showing the power flow within the engine for the Mach 0.75 point. The numbers are the power transfer in kW.

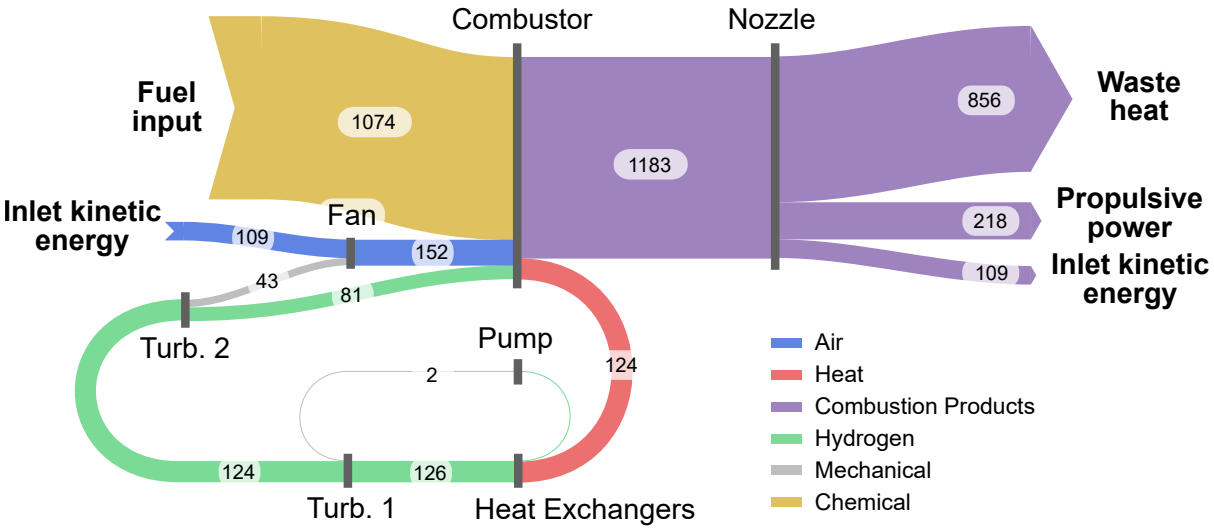

Fig 13. Sankey diagram showing the power flow within the engine for the Mach 2.00 point. The numbers are the power transfer in kW.

4. Conclusion and Future Work

An uninstalled off-design transient model of an expander-type air-turbo-rocket (ATR) was used to explore the engine performance, controllability, transient behaviour, and turbomachinery limitations. The control strategy consisted of adding two turbine bypass valves, which control the throttle parameters using PI controllers. This strategy was proven to be successful in controlling the engine in the explored section of the flight trajectory and was shown to provide a means of engine thrust throttling. The turbomachinery off-design behaviour and the implemented control strategy has shown to lead to a different engine performance compared to previously used on-design simulations, highlighting the importance of taking the turbomachinery off-design behaviour into account. The model was further exploited to investigate transient engine behaviour. When applying thrust step inputs, a strong hysteresis effect has been identified, which is similar to conventional turbo-based cycles. Some limitations of the current model have been identified. First, the matching of the turbomachinery components proved to be difficult. Especially the operational range of the turbines concerning their corrected mass flow rate proved to be a limiting factor. Replacing the turbomachinery maps with more representative ones could alleviate this issue. Secondly, this work only investigates one of the possible control strategies. Other control strategies should be explored in the future, which could have benefits for engine efficiency and controllability. Thirdly, this ATR is conceived as part of a combined-cycle engine to power a supersonic passenger aircraft. This would change the nozzle and heat exchanger topology, which have been simplified in this study.

Acknowledgements

This project has received funding from the H2020 MOREandLESS project under grant agreement number 101006856.

References

[1] I. Rodríguez-Miranda, V. Fernández-Villacé, and G. Paniagua. "Modelling, Analysis, and Optimization of the Air-Turborocket Expander Engine". In: *Journal of Propulsion and Power* 29.6 (Nov. 2013), pp. 1266–1273.

[2] V. Fernández-Villacé and G. Paniagua. "On the Exergetic Effectiveness of Combined-Cycle Engines for High Speed Propulsion". In: *Energy* 51 (Mar. 2013), pp. 382–394.

[3] V. Balepin. "High Speed Propulsion Cycles". In: *Advances on Propulsion Technology for High-Speed Aircraft* (2008).

[4] F. Jivraj et al. "The Scimitar Precooled Mach 5 Engine". In: *2ND EUROPEAN CONFERENCE FOR AEROSPACE SCIENCES*. 2007.
[5] Hiroaki Kobayashi et al. "Development Status of Mach 6 Turbojet Engine in JAXA". In: *55th International Astronautical Congress of the International Astronautical Federation, the International Academy of Astronautics, and the International Institute of Space Law*. Vancouver, British Columbia, Canada: American Institute of Aeronautics and Astronautics, Oct. 2004.
[6] J. Steelant and T. Langener. "THE LAPCAT-MR2 HYPERSONIC CRUISER CONCEPT". In: *29th Congress of the International Council of the Aeronautical Sciences*. Moscow, 2014.
[7] T. Langener, S. Erb, and J. Steelant. "TRAJECTORY SIMULATION AND OPTIMIZATION OF THE LAPCAT-MR2 HYPERSONIC CRUISER CONCEPT". In: *29th Congress of the International Council of the Aeronautical Sciences*. St. Petersburg, Russia, July 2014.
[8] N. Viola et al. "Main Challenges and Goals of the H2020 STRATOFLY Project". In: *Aerotecnica Missili & Spazio* 100.2 (June 2021), pp. 95–110.
[9] N. Viola et al. "HYPERSONIC AIRCRAFT AND MISSION CONCEPT RE-DESIGN TO MOVE FROM MACH 8 TO MACH 5 OPERATIONS". In: *33rd Congress of the International Council of the Aeronautical Sciences*. Stockholm, Sweden, Sept. 2022.
[10] R. Fusaro et al. "Economic and Environmental Sustainability of Liquid Hydrogen Fuel for Hypersonic Transportation Systems". In: *CEAS Space Journal* 12.3 (Sept. 2020), pp. 441–462.
[11] V. Fernández-Villacé, G. Paniagua, and J. Steelant. "Installed Performance Evaluation of an Air Turbo-Rocket Expander Engine". In: *Aerospace Science and Technology* 35 (May 2014), pp. 63–79.
[12] P. M. Goncalves, A. C. Ispir, and B. H. Saracoglu. "Development and Optimization of a Hypersonic Civil Aircraft Propulsion Plant with Regenerator System". In: *AIAA Propulsion and Energy 2019 Forum*. Indianapolis, IN: American Institute of Aeronautics and Astronautics, Aug. 2019.
[13] A. C. Ispir, B. O. Cakir, and B. H. Saracoglu. "Design Space Exploration for a Scramjet Engine by Using Data Mining and Low-Fidelity Design Techniques". In: *2nd International Conference on High-Speed Vehicle Science & Technology*. Bruges, Belgium: Council of European Aerospace Societies, 2022.
[14] Emoresarios Agrupados. *EcosimPro User Manual*. 2013.
[15] L. Petzhold. "A Description of DASSL: A Differential/Algebraic System Solver". In: *Proc. 10th IMACS World Congress*. 1982.
[16] J. Moral et al. *ESPSS SIMULATION PLATFORM*. 2010.
[17] S. Gordon and B. J. McBride. *Computer Program for Calculation of Complex Chemical Equilibrium Compositions and Applications*. Tech. rep. Reference publication 1311. National Aeronautics and Space Administration, Oct. 1994.
[18] E. Lemmon, M. McLinden, and M. Huber. *NIST Standard Reference Database23: Reference Fluid Thermodynamic and Transport Properties - REFPROP, Version 7.0. National Institute of Standards and Technology, Standard Reference Data Program.* 2002.
[19] V. Fernández Villacé. "Simulation, Design and Analysis of Air-Breathing Combined-Cycle Engines for High Speed Propulsion". PhD thesis. Universidad Politécnica de Madrid, 2013.
[20] T. Verstraete. "CADO: A Computer Aided Design and Optimization Tool for Turbomachinery Applications". In: *2nd International Conference on Engineering Optimization*. Lisbon, Portugal, 2010.
[21] K. Deb and H. Jain. "An Evolutionary Many-Objective Optimization Algorithm Using Reference-Point-Based Nondominated Sorting Approach, Part I: Solving Problems With Box Constraints". In: *IEEE Transactions on Evolutionary Computation* 18.4 (Aug. 2014), pp. 577–601.
[22] P. J. Huber and E. M. Ronchetti. *Robust Statistics*. 2nd ed. Wiley Series in Probability and Statistics. Hoboken (N.J.): Wiley, 2009.
[23] J. Bossard and M. Thomas. "The Influence of Turbomachinery Characteristics on Air Turbo Rocket Engine Operation". In: *36th AIAA/ASME/SAE/ASEE Joint Propulsion Conference and Exhibit*. Las Vegas,NV,U.S.A.: American Institute of Aeronautics and Astronautics, July 2000.
[24] G. Converse and R. Giffin. *Extended Parametric Representation of Compressors, Fans and Turbines - Vol. I - CMGEN User's Manual*. Tech. rep. NASA CR-174645. 1983.

[25] R. G. Stabe, W. J. Whitney, and T. P. Moffitt. "Performance of a High-work Low Aspect Ratio Turbine Tested with a Realistic Inlet Radial Temperature Profile". In: *Joint Propulsion Conference*. Cincinnati Ohio, 1984.
[26] E. Wylie, V. Streeter, and L. Suo. *Fluid Transients in Systems*. Prentice Hall, Inc, 1993.
[27] J. Sivadasan et al. "Design of Cross-Coupled Nonlinear PID Controller Using Single-Objective Evolutionary Algorithms". In: *Mathematical Problems in Engineering* 2023 (Apr. 2023). Ed. by X. Shao, pp. 1–13.
[28] J. G. Ziegler and N. B. Nichols. "Optimum Settings for Automatic Controllers". In: *Transactions of the ASME* (1942), pp. 759–768.